Decentralized Frequency Restoration and Power Oscillation Damping Control for Islanded Microgrids with Multiple VSGs

Xueping Li, Sheng Huang, Zili Wang, Zhijie Lian, Yinpeng Qu, Yandong Chen, and Derong Luo

***Abstract*—Traditional virtual synchronous generator (VSG) suffers from frequency steady-state deviation in islanded microgrids, which negatively affects the frequency-sensitive loads. Moreover, similar to the synchronous generator, VSG introduces active power oscillation, especially under the condition of multiple parallel VSGs, which may cause overload or damage to the VSG because of its low overcurrent capability as a power electronic inverter. To address these issues, a decentralized frequency restoration and power oscillation damping control method is proposed in this paper, in which the global variable characteristic of the microgrid frequency is considered to restore it to the rated value while ensuring precise active power sharing. Moreover, the proposed control method can dampen the power oscillation during load disturbance without affecting the steady-state characteristics. In addition, the fully decentralized manner obviates the requirement for communication networks, thereby considerably reducing the communication burden and improving system reliability. Finally, simulations and experiments are conducted to validate the effectiveness of the proposed control method.**

***Index Terms*—Microgrid, virtual synchronous generator (VSG), oscillation, frequency restoration, power sharing, damping control.**

I. Introduction

With the increasing penetration rate of new energy and the application of numerous power electronic converters in islanded microgrids, the islanded microgrid faces severe instability risk due to its low inertia, weak damping characteristics, and lack of stable frequency and voltage support from the large power grid [1], [2]. Virtual synchronous generator (VSG) provides a promising solution to enhance the stability of islanded microgrid dominated by power electronic converters as it emulates the dynamic characteristics of the synchronous generator (SG) to ensure inverters possess favorable features such as inertia and damping [3]-[5].

However, traditional VSG control induces steady-state deviation in the frequency [6]. When subjected to heavy load switching, the steady-state deviation of frequency may exceed the boundary, thus seriously affecting the operation of the frequency-sensitive loads and even leading to adverse effects on system stability. Moreover, owing to the similarities in mechanical and electromagnetic equations with SG, an islanded microgrid containing multiple VSGs in parallel may suffer from active power oscillation during load fluctuations. Since the VSG is a power semiconductor device with weak overcurrent capability, it might be damaged when subjected to active power oscillation [7], [8]. Therefore, both secondary frequency regulation and active power oscillation suppression should be achieved in an islanded microgrid containing multiple VSGs during load disturbance.

Various techniques are proposed to compensate for the steady-state frequency deviations in traditional VSG control. The majority of existing secondary frequency control methods are based on communication infrastructures to achieve frequency restoration, which can be divided into two categories, namely, centralized and distributed secondary control methods. Particularly, in [9] and [10], the frequency is restored to the rated value in a centralized manner. However, due to the heavy communicational burden and high dependence on point-to-point communication, the major drawbacks of centralized control methods include single point of failure, low scalability, and low flexibility.

To alleviate the communication burden, plenty of distributed secondary frequency control methods using a sparse communication network are suggested. In [11], a distributed secondary frequency control method is presented to eliminate the frequency deviations by utilizing a significantly high bandwidth. Further, [12] presents a distributed robust finite-time secondary control for frequency restoration and accurate active power sharing using only a sparse communication network to exchange information among neighboring distributed generators. In [13], frequency regulation and active power sharing are ensured by switching between distributed droop-free and standard frequency droop controls under the conditions of electrical and communication failures; however, the complicated switched control policy is the main constraint. In [14], frequency deviations are compensated using

Manuscript received: March 8, 2024; revised: June 9, 2024; accepted: August 9, 2024. Date of CrossCheck: August 9, 2024. Date of online publication: August 26, 2024.

This work was supported by the National Key Research and Development Program of China (No. 2022YFF0608700).

X. Li, S. Huang, Z. Wang, Z. Lian (corresponding author), Y. Qu, Y. Chen, and D. Luo are with the College of Electrical and Information Engineering, Hunan University, Changsha, China (e-mail: lxp1993@hnu.edu.cn; huang98123@163.com; zili_wang666@hnu.edu.cn; zhijie003@hnu.edu.cn; quyinpeng@hnu.edu.cn; yandong_chen@hnu.edu.cn; hdldr@hnu.edu.cn).

DOI: 10.35833/MPCE.2024.000255

iterative learning mechanics, while ensuring accurate active power sharing in a distributed manner. In [15], a distributed consensus-based control method based on H_∞ theory is proposed to regulate microgrid frequency to track frequency set points and provide accurate active power sharing; however, its main drawback is the complicated design procedure of the H_∞ protocol. To further reduce information exchange and communication bandwidth, some even-trigger-based secondary control methods are presented in [16]-[21]. In [19], a distributed secondary frequency control method is proposed to achieve frequency restoration under event-triggered communication. Although these methods can address issues related to communication uncertainties in terms of data drop-out and communication time delay, the system must be constantly monitored to determine the action. Moreover, the complexity of the design procedure for the event-triggered rules is the main limitation of these methods. In summary, the performance of the aforementioned centralized and distributed secondary control methods is inevitably susceptible to failures of communication link.

To eliminate the need for communication networks, some decentralized methods characterized by no communication have emerged recently. In [22], the steady-state frequency deviation of the microgrid is compensated using a linear quadratic regulator (LQR) in a decentralized manner. Nevertheless, it fails to keep the desired power sharing ratio, and the complexity of optimal LQR design is the constraint in practical implement. In [23], a secondary frequency regulation control method on the basis of a switched control method and a time-dependent protocol is proposed; however, the utilization of event-detection and time-dependent protocols increases the control complexity and implementation difficulty, which may adversely affect the system stability and reliability. An estimation-based consensus solution employing active power estimation is proposed in [24], which utilizes a communication-less structure and targets frequency regulation and accurate active power sharing problems in islanded microgrids. In [25], secondary frequency regulation is achieved by introducing a simplified bandpass washout filter, which is composed by cascading a high-pass filter and a low-pass filter. In [26], a decentralized control method is introduced for frequency restoration and active power sharing; however, whether this method is capable of suppressing active power oscillation is not discussed, since obvious active power oscillation can still be observed during load disturbance.

Motivated by the aforementioned efforts, a fully decentralized frequency restoration and power oscillation damping control method is proposed to achieve frequency restoration accompanied with the precise active power sharing function as well as active power oscillation suppression in islanded microgrids containing multiple VSGs in parallel. Particularly, in contrast to the existing decentralized secondary frequency control methods, the proposed control method in this paper provides the following salient features.

1) In the design procedure, the proposed control method takes advantage of the unique characteristic of the microgrid frequency as a global variable in steady state to eliminate the steady-state deviation of the microgrid frequency and achieve precise active power sharing.

2) The proposed control method is implemented in a totally communication-free decentralized manner. During load fluctuations, frequency deviation-free regulation control with precise active power sharing function operates synergistically with the transient damping enhancement control to achieve frequency restoration accompanied with active power sharing function as well as active power oscillation suppression without using any communication links.

3) In comparison to the conventional decentralized secondary frequency control presented in [26], the proposed control method enhances system reliability by suppressing active power oscillation during load disturbance. In other words, the proposed control method guarantees active power sharing in both steady-state and transient scenarios.

4) In comparison to classical control methods, the proposed control method boasts several notable advantages, including straightforward parameter design, simplified implementation, and enhanced flexibility that facilitates plug-and-play functionality without the need for redesign.

The rest of this paper is organized as follows. Section II presents the problems associated with the traditional VSG active power control loop. Section III describes the proposed control method. The design of key parameters and stability analysis are presented in Section IV. Simulation and experimental results are provided in Section V and Section VI, respectively. Finally, the conclusions are given in Section VII.

II. Problems of Traditional VSG Active Power Control Loop

A. Traditional VSG Active Power Control Algorithm

A typical VSG topology is shown in Fig. 1. L_f and C_f are the filter inductance and filter capacitance, respectively; L_{line} is the line inductance; i_L is the inverter-side current; i_o and u_o are the VSG output current and voltage, respectively; P_m and Q_{ref} are the mechanical power and reactive power reference, respectively; U_{nom} and E are the root-mean-square (RMS) values of the rated voltage and inner electric potential of the VSG, respectively; D_p and D_q are the damping and the voltage-drooping coefficients, respectively; J_ω is the inertia coefficient; θ is the internal voltage phase angle of VSG; ω_0 is the rated angular frequency; K_q is the reactive power regulation inertia coefficient; and U_{bus} is the three-phase grid voltage.

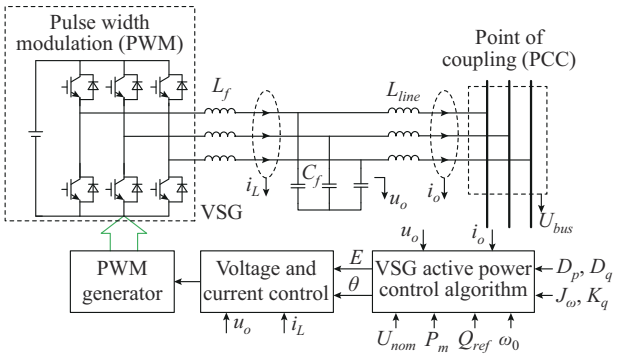

Fig. 1. Typical VSG topology.

The traditional VSG active power control is shown in Fig. 2 [27]. The active power controller of the VSG emulates the inertia and primary frequency regulations of the SG, and the reactive power controller simulates the primary voltage regulation of the SG. The mathematical equations can be expressed as:

$$\begin{cases} \dfrac{P_m}{\omega_0} - \dfrac{P_e}{\omega_0} + D_p(\omega_0 - \omega) = J_\omega \dfrac{\mathrm{d}\omega}{\mathrm{d}t} \\ Q_{ref} - Q_e + \sqrt{2}\, D_q(U_{nom} - U_o) = K_q \dfrac{\mathrm{d}E}{\mathrm{d}t} \end{cases} \tag{1}$$

where ω is the VSG output angular frequency; U_o is the RMS value of the output voltage of the VSG; and P_e and Q_e are the output active power and reactive power, respectively, which can be calculated using the instantaneous power theory.

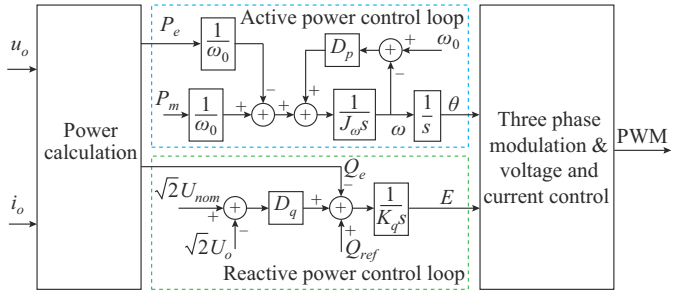

Fig. 2. Traditional VSG active power control.

B. Problem of Steady-state Frequency Deviation

According to (1), when the load changes, the VSG output frequency can be expressed as:

$$\omega(t) = \omega_0 - \frac{P_m - P_e}{D_p \omega_0}\left(1 - \mathrm{e}^{-\frac{D_p}{J_\omega}t}\right) = \omega_0 - \frac{\Delta P_L}{D_p \omega_0}\left(1 - \mathrm{e}^{-\frac{D_p}{J_\omega}t}\right) \tag{2}$$

where ΔP_L is the load variation.

According to (2), the steady-state deviation of VSG frequency can be expressed as:

$$\lim_{t\to\infty}\left|\Delta\omega(t)\right| = \lim_{t\to\infty}\left|\omega(t) - \omega_0\right| = \frac{\Delta P_L}{D_p \omega_0} \neq 0 \tag{3}$$

Hence, (3) implies that the system frequency cannot return to its rated value when the system suffers from load disturbance. In an islanded microgrid, heavy load disturbance may cause significant steady-state deviation from rated system frequency, resulting in some frequency-sensitive loads not working properly. Therefore, VSG needs to have the capability for secondary frequency regulation.

C. Mechanism of Active Power Oscillation

The equivalent circuit diagram of two parallel VSGs in an islanded microgrid is shown in Fig. 3. In Fig. 3, E_i ($i = 1, 2$) represents the output voltage amplitude of VSGi; δ_i represents the power angle of VSGi; ω_i represents the output angular frequency of VSGi; P_{ei} represents the output active power of VSGi; X_{si} represents the output impedance of VSGi; X_{linei} represents the line impedance of VSGi; X_{ti} represents the impedance that includes both the output impedance X_{si} and line impedance X_{linei}, i.e., $X_{ti} = X_{si} + X_{linei}$; and $Z_L \angle \theta_L$ represents the load impedance.

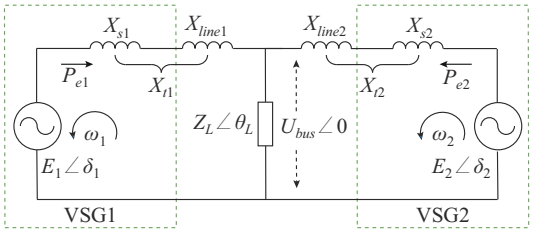

Fig. 3. Equivalent circuit diagram of two parallel VSGs.

To simplify the analysis, the inertia coefficient and damping coefficient of the two VSGs are assumed to be equal, i.e., $J_{\omega 1} = J_{\omega 2}$ and $D_{p1} = D_{p2}$. Meanwhile, the line impedance is inductive and the phase difference between the two VSGs is extremely small, which can be estimated as $\sin(\delta_1 - \delta_2) = \delta_1 - \delta_2$, $\cos(\delta_1 - \delta_2) = 1$. Therefore, the small-signal model can be obtained as:

$$\begin{cases} \Delta P_{e1} = \dfrac{3E_1E_2}{X_{t1}X_{t2}M}\sin(\Delta\delta_2 - \Delta\delta_1)\sin\theta_M \\ \Delta P_{e2} = \dfrac{3E_1E_2}{X_{t1}X_{t2}M}\sin(\Delta\delta_1 - \Delta\delta_2)\sin\theta_M \end{cases} \tag{4}$$

$$M\angle\theta_M = \frac{1}{X_{t1}\angle 90^\circ} + \frac{1}{X_{t2}\angle 90^\circ} + \frac{1}{Z_L\angle\theta_L} \tag{5}$$

where M is the magnitude of system impedance; and θ_M is the phase of system impedance. Let $\Delta\omega = \omega_1 - \omega_2$ and $\Delta\delta = \delta_1 - \delta_2$ be state variables. By combining (1) and (4), we can obtain:

$$\begin{bmatrix} \Delta\dot{\omega} \\ \Delta\dot{\delta} \end{bmatrix} = \begin{bmatrix} -\dfrac{D_p}{J_\omega} & \dfrac{6E_1E_2\sin\theta_M}{J_\omega\omega_0X_{t1}X_{t2}M} \\ 1 & 0 \end{bmatrix}\begin{bmatrix} \Delta\omega \\ \Delta\delta \end{bmatrix} \tag{6}$$

The closed-loop pole distribution diagram of parallel VSGs under different inertia coefficients is shown in Fig. 4.

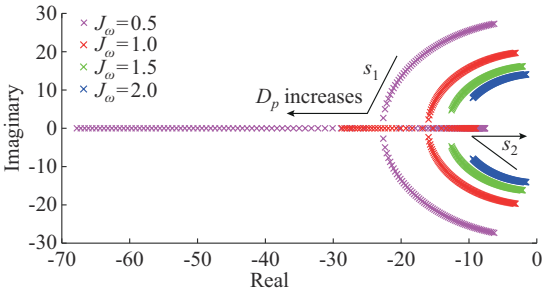

Fig. 4. Closed-loop pole distribution diagram of parallel VSGs.

As shown in Fig. 4, a pair of conjugate complex poles, designated as s_1 and s_2, moves towards the negative real axis and eventually split into two different negative real poles as D_p increases, which means the system shifts from under-damping to over-damping, being able to suppress the active power oscillation under load fluctuation. When D_p is constant, the larger the value of J_ω, the closer the poles are to the imaginary axis, indicating that the system is more prone to active power oscillation. However, it is not advisable to directly adjust the inertia and damping coefficients of the VSG to suppress active power oscillation, since small J_ω is not conducive to the system frequency stability and changing D_p affects the steady-state characteristics of the system.

III. Proposed Control Method

As shown in Fig. 5, the proposed control method consists of two parts, i.e., frequency restoration control with precise active power sharing function and transient damping enhancement control. The detailed mechanism of the proposed control method is presented in the following subsections.

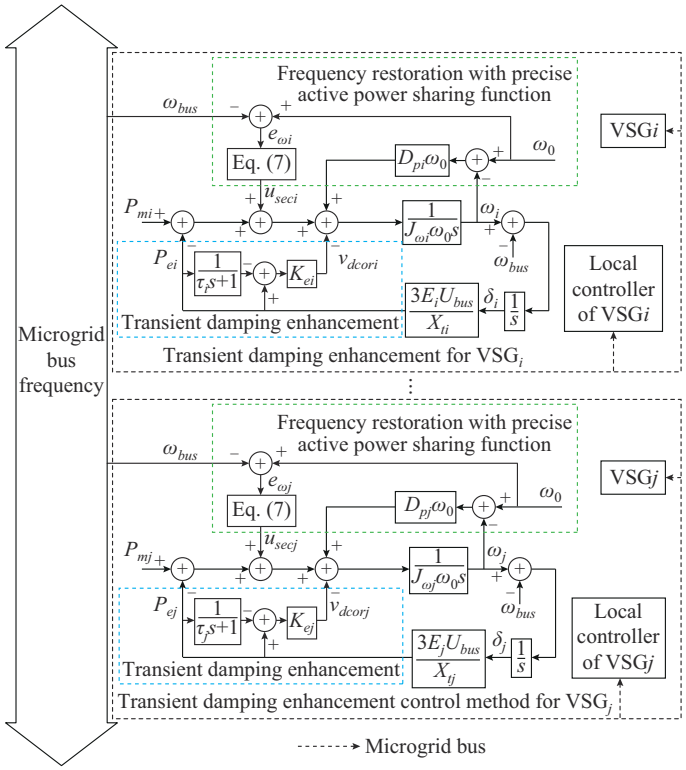

Fig. 5. Overall control diagram of proposed control method.

A. Analysis of Frequency Restoration Control

The frequency restoration control u_{sec} can be expressed as:

$$u_{sec} = a\int(\omega_0 e_\omega - b u_{sec})\mathrm{d}t \tag{7}$$

where $e_\omega = \omega_0 - \omega_{bus}$ is the steady-state frequency error, and ω_{bus} is the bus frequency; and a and b are the constants, and the value of a is proportional to the rated power of VSG.

According to Fig. 5, under the proposed control method, the active power characteristics of VSGi can be expressed as:

$$\frac{P_{mi}}{\omega_0} - \frac{P_{ei}}{\omega_0} + D_{pi}(\omega_0 - \omega_i) + \frac{u_{seci}}{\omega_0} - \frac{v_{dcori}}{\omega_0} = J_{\omega i}\frac{\mathrm{d}\omega_i}{\mathrm{d}t} \tag{8}$$

where v_{dcori} is the damping enhancement control; and the subscript i denotes the i^{th} VSG.

Since the transient damping enhancement control does not work in a steady state (as explained below), and the frequency of each VSG is equal to the bus frequency in the steady state, according to (7) and (8), it can be concluded that:

$$e_\omega = \frac{P_m - P_e}{J_\omega\omega_0 s + \dfrac{a\omega_0}{s+ab} + D_p\omega_0} = \frac{P_m - P_e}{\omega_0(D_p + 1/b)} \tag{9}$$

If b is greater than 0 and far less than 1, and let b equal b/D_p, then according to (9), (10) can be further obtained as:

$$e_\omega = \omega_0 - \omega_{bus} = \frac{P_m - P_e}{\omega_0 D_p/b} = 0 \tag{10}$$

Therefore, when the system is in a steady state, $e_\omega = 0$, i.e., $\omega_{bus} = \omega_0$, indicating that the proposed control method can restore the microgrid frequency to its rated value.

B. Analysis of Transient Damping Enhancement Control

To effectively solve the issue of active power oscillation during load disturbance, the transient damping enhancement control is introduced, which can be expressed as:

$$v_{dcori} = \frac{K_{ei}\tau_i s}{\tau_i s + 1} P_{ei} \tag{11}$$

where τ_i is the time period; and K_{ei} is the parameter.

The operation principle of damping improvement is that, v_{dcori} is obtained by multiplying K_{ei} with a high pass filter with a reasonable cutoff frequency f_c. The fundamental idea behind (11) is to compensate for the damping power that only exists during load disturbance, thus improving the transient damping characteristics of VSGi and enhancing the system ability in terms of active oscillation suppression without affecting the steady-state characteristics of VSGi.

According to (1) and (11), after introducing the transient damping enhancement control module, the damping ratio ξ_i of VSGi can be expressed as:

$$\xi_i = \frac{D_{pi}\omega_0 + K_i K_{ei}\tau_i + K_i\tau_i}{2\sqrt{(J_{\omega i}\omega_0 + D_{pi}\omega_0\tau_i)K_i}} \tag{12}$$

The root locus is applied to visually demonstrate the relationship between the characteristic roots and each of K_e and τ, as shown in Fig. 6.

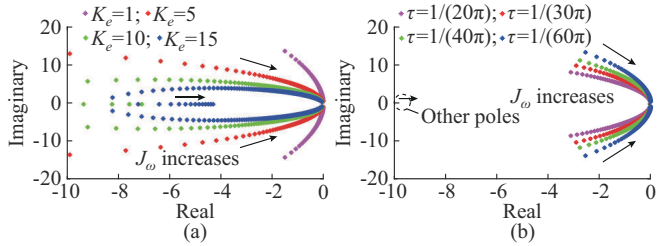

Fig. 6. Dominant pole distribution when J_ω increases under different parameters. (a) K_e. (b) τ.

Figure 6(a) shows the dominant pole distribution when J_ω increases under different K_e. Under the same J_ω, the system damping enhances with the increase of K_e, suggesting that the large K_e is beneficial to the active power oscillation. Additionally, as shown in Fig. 6(b), since τ is a time constant of the filter, a reasonable cutoff frequency should be determined to ensure the effective extraction of power oscillation components; thus, the adjustment range of τ is limited. Moreover, it is worth noting that τ has a relatively minimal effect on system damping than K_e. In other words, K_e has a dominant impact on system damping.

C. Frequency Restoration Control with Precise Active Power Sharing

By introducing parameter μ and assuming that $b = c\mu^{-1}$, (9) can be rewritten as:

$$e_\omega = \omega_0 - \omega_{bus} = \frac{P_m - P_e}{\omega_0 (D_p + 1/b)} = \frac{P_m - P_e}{\omega_0 (D_p + \mu/c)} \tag{13}$$

When the system reaches the steady state, since the frequency of the microgrid is globally consistent, (14) can be obtained.

$$e_{\omega i} = \frac{P_{mi} - P_{ei}}{\omega_n (D_{pi} + \mu_i / c_i)} = \frac{P_{mj} - P_{ej}}{\omega_n (D_{pj} + \mu_j / c_j)} = e_{\omega j} \tag{14}$$

where the subscript j denotes the j^{th} VSG.

If $\mu_i = D_{pi}$, the following equation can be obtained:

$$e_{\omega i} = \frac{P_{mi} - P_{ei}}{\omega_n D_{pi} (1 + 1/c_i)} = \frac{P_{mj} - P_{ej}}{\omega_n D_{pj} (1 + 1/c_j)} = e_{\omega j} \tag{15}$$

If c is greater than 0 and far less than 1, and $c_i = c_j$, then $e_{\omega i} = e_{\omega j} \approx 0$. Generally, the value of damping coefficient D_p is proportional to the rated power of VSG, i.e.,

$$P_{mi} : P_{mj} = D_{pi} : D_{pj} = a_i : a_j = \alpha_i : \alpha_j \tag{16}$$

Thus, according to (15) and (16), (17) can be obtained as:

$$\frac{P_{ei}}{D_{pi}(1 + 1/c_i)} = \frac{P_{ej}}{D_{pj}(1 + 1/c_j)} \tag{17}$$

By extending (17) to the system containing multiple VSGs, the following equation can be obtained as:

$$P_{e1} : P_{e2} : \ldots : P_{en} = D_{p1}(1 + 1/c_1) : D_{p2}(1 + 1/c_2) : \ldots : D_{pn}(1 + 1/c_n) \tag{18}$$

Since $c_1 = c_2 = \ldots = c_n$, (18) can be further deduced as:

$$P_{e1} : P_{e2} : \ldots : P_{ei} : \ldots : P_{en} = D_{p1} : D_{p2} : \ldots : D_{pi} : \ldots : D_{pn} \tag{19}$$

By combining (18) and (19), (20) can be obtained.

$$P_{e1} : P_{e2} : \ldots : P_{ei} : \ldots : P_{en} = \alpha_1 : \alpha_2 : \ldots : \alpha_i : \ldots : \alpha_n \tag{20}$$

In summary, the proposed control method achieves frequency restoration and precise allocation of active power without requiring any timing coordination between the two functions.

IV. Design of Key Parameters and Stability Analysis

This section investigates the impact of the proposed control method on system stability. A small-signal model of the system containing three VSGs is established, as shown in Fig. 7.

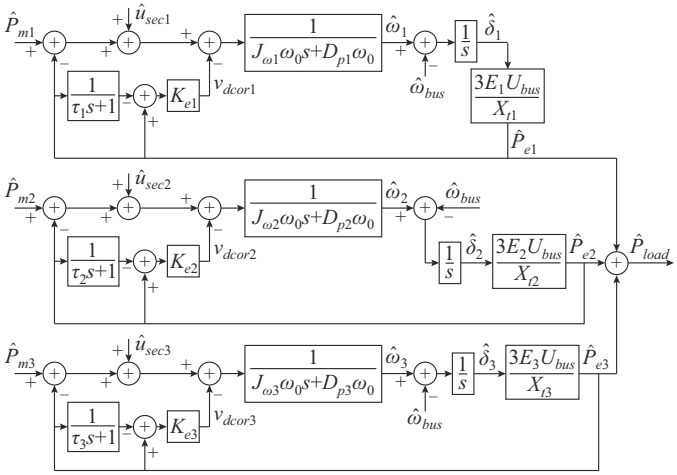

Fig. 7. Small-signal model of system when using proposed control method.

Let $J_i = J_{\omega i}\omega_0$ and $D_i = D_{pi}\omega_0$, then (8) can be rewritten as:

$$J_i \frac{\mathrm{d}\omega_i}{\mathrm{d}t} = P_{mi} - P_{ei} + D_i(\omega_0 - \omega_i) - u_{dcori} + u_{seci} \tag{21}$$

From the law of energy conservation, the following equation can be obtained:

$$K_1\hat{\delta}_1 + K_2\hat{\delta}_2 + K_3\hat{\delta}_3 = \hat{P}_{load} \tag{22}$$

where $\hat{}$ denotes the small variation of each variable.

Then, the system state-space model can be expressed as:

$$\begin{cases} \dot{\boldsymbol{x}} = \boldsymbol{A}\boldsymbol{x} + \boldsymbol{B}\boldsymbol{u} \\ \dot{\boldsymbol{y}} = \boldsymbol{C}\boldsymbol{x} + \boldsymbol{D}\boldsymbol{u} \end{cases} \tag{23}$$

$$\boldsymbol{A} = \begin{bmatrix} \boldsymbol{A}_1 & \boldsymbol{A}_2 \\ \boldsymbol{A}_3 & \boldsymbol{A}_4 \end{bmatrix} \tag{24}$$

$$\boldsymbol{x} = [\hat{\omega}_1 \quad \hat{\omega}_2 \quad \hat{\omega}_3 \quad \hat{\delta}_1 \quad \hat{\delta}_2 \quad \hat{x}_{p1} \quad \hat{x}_{p2} \quad \hat{x}_{p3} \quad \hat{x}_{\omega 11} \quad \hat{x}_{\omega 12} \quad \hat{x}_{\omega 13} \quad \hat{x}_{\omega 21} \quad \hat{x}_{\omega 22} \quad \hat{x}_{\omega 23} \quad \hat{x}_{\omega 31} \quad \hat{x}_{\omega 32} \quad \hat{x}_{\omega 33}] \tag{25}$$

$$\boldsymbol{u} = [\hat{P}_{m1} \quad \hat{P}_{m2} \quad \hat{P}_{m3} \quad \hat{P}_{load}] \tag{26}$$

$$\boldsymbol{y} = [\hat{\omega}_1 \quad \hat{\omega}_2 \quad \hat{\omega}_3 \quad \hat{P}_{e1} \quad \hat{P}_{e2} \quad \hat{P}_{e3}] \tag{27}$$

where the added variables x_{pi} and $x_{\omega ij}$ represent the state variables introduced by the proposed control method in the three VSGs, respectively, and their expressions can be respectively depicted as:

$$\begin{cases} \hat{x}_{pi} = \dfrac{\hat{P}_{ei}}{\tau_i s + 1} \\ \hat{x}_{\omega ij} = \dfrac{a_i \omega_0 \hat{\omega}_j}{s + a_i b_i} \end{cases} \tag{28}$$

The expressions of other matrices such as $\boldsymbol{A}_1$, $\boldsymbol{A}_2$, $\boldsymbol{A}_3$, $\boldsymbol{A}_4$, $\boldsymbol{B}$, $\boldsymbol{C}$, and $\boldsymbol{D}$ are shown in the Supplementary Material A, and $\boldsymbol{O}_{x \times y} = zeros(x, y)$ indicates an $x \times y$ matrix of zeros.

Next, the sensitivity analysis is conducted to determine appropriate ranges for system key control parameters such as a, b, K_e, and τ.

Figure 8 shows the locus of the dominant poles when a changes from 1 to 1190 under different K_e. Although under different K_e, when a is approximately equal to 1039, the eigenvalues enter the right-half s plane, resulting in system instability. Consequently, the maximum value of a that maintains the system stability is approximately 1039. Therefore, to guarantee system stability under different K_e, $a_i (i = 1, 2, \ldots)$ of VSGi should be less than 1039. Additionally, as evident in Fig. 8, it can be concluded that K_e has almost no impact on the selection range of a.

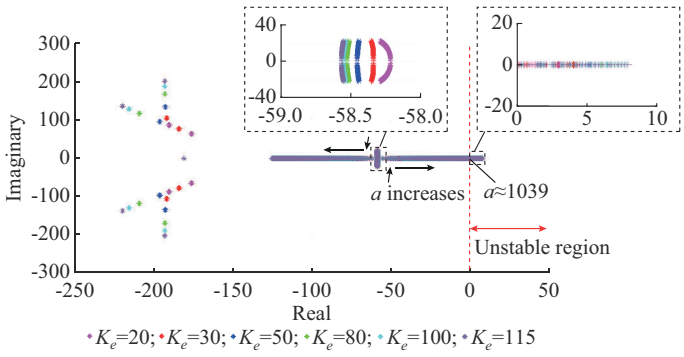

Fig. 8. Locus of dominant poles when a increases under different K_e.

Figure 9 shows the locus of dominant eigenvalues when b changes from 1×10^{-6} to 1×10^{-4}. In fact, according to the eigenvalue locus shown in Fig. 8 and Fig. 9, on the premise of system stability, the selection margin of a and b is relatively sufficient. Therefore, a and b of different VSGs can be designed according to the theoretical analysis presented in Section III.

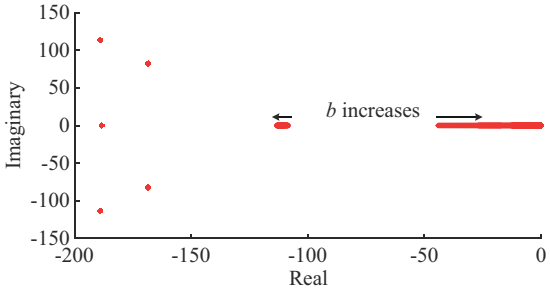

Fig. 9. Locus of dominant eigenvalues when b changes.

Figure 10 shows system dominant poles when K_e increases from 0.1 to 100 under different τ. Under the same value of K_e, a large time constant τ is conducive to dampening power oscillation to a small extent. However, it is still necessary to compromise between the damping effect and time delay since larger τ results in longer time delay. Therefore, based on the aforementioned analysis, τ is selected to be $1/(30\pi)$.

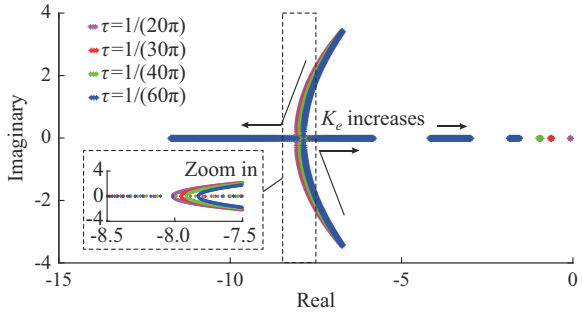

Fig. 10. System dominant poles when K_e increases under different τ.

Additionally, as K_e increases, a pair of conjugate poles meets each other on the real axis and constitutes a new pair of negative real poles, which means the system damping is enhanced. Hence, a large K_e helps suppress the active power oscillation. However, K_e is not supposed to be too large, since there is a risk of poles crossing the imaginary axis to the right half plane with the further increase of K_e, resulting in system instability. As illustrated in Fig. 11, the maximum value of K_e that maintains system stability is approximately 132.

Figure 12 shows system dominant poles when J_ω changes from 0.01 to 10 under different K_e. As clearly presented in Fig. 12, under the same J_ω, the damping of the system with large K_e is greater than that of the system with small K_e, indicating that the large K_e can contribute greater damping to suppress the active power oscillation, which is consistent with the conclusion conducted in Fig. 10.

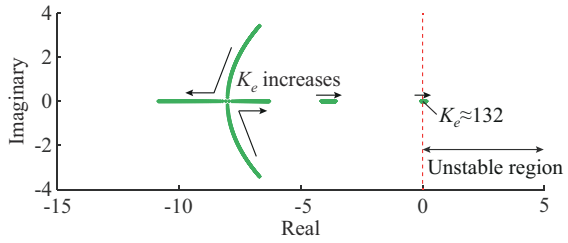

Fig. 11. System dominant pole distribution when K_e increases from 0.1 to 150.

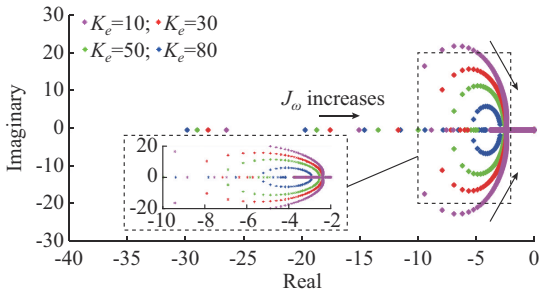

Fig. 12. System dominant poles when J_ω changes under different K_e.

Consequently, based on the analysis of the impact of K_e on the system stability in Figs. 10-12, trade-offs should be made between the aforementioned principles. Accordingly, K_e is selected to be 50.

V. Simulation Verification

To verify the effectiveness of the proposed control method, simulations are conducted using MATLAB/Simulink. To achieve more general simulation results, different VSGs adopt different inertia and damping coefficients. The ratio of rated capacities of VSG1, VSG2, and VSG3 is 1:2:3, and the system load is 60 kW at the initial moment. System parameters are shown in Table I.

TABLE I
System Parameters

Parameter ($i=1, 2, 3$)	VSG1	VSG2	VSG3
L_{fi}	3 mH	3 mH	3 mH
C_{fi}	50 μF	50 μF	50 μF
L_{line}	1.5 mH	3.2 mH	2.4 mH
$J_{\omega i}$	1	3	5
D_{pi}	20	40	60
U_{nomi}	220 V	220 V	220 V
K_{qi}	100	100	100
a_i	200	400	600
b_i	$5\times10^{-5}/2$	$5\times10^{-5}/4$	$5\times10^{-5}/6$
K_{ei}	50	50	50
τ_i	$1/(30\pi)$	$1/(30\pi)$	$1/(30\pi)$
ω_0	100π rad/s	100π rad/s	100π rad/s

A. Case A: Comparisons with Different Control Methods

In this case, to show the merits of the proposed control method, different control methods are adopted for compara-

tive testing, and a 53 kW load is added at $t=5$ s.

The traditional VSG control is implemented as a benchmark, and the corresponding simulation results are shown in Fig. 13. As it can be observed, when the traditional VSG control method is utilized, both the frequency steady-state deviations and severe active power oscillation phenomenon occur in the case of sudden load changes. Moreover, the maximum peak power of VSG1, VSG2, and VSG3 is 30.58 kW, 41.8 kW, and 62.8 kW, respectively, with an oscillation period of approximately 2.2 s. Additionally, the system frequency f_{bus} significantly deviates from its rated value, as shown in Fig. 13(b).

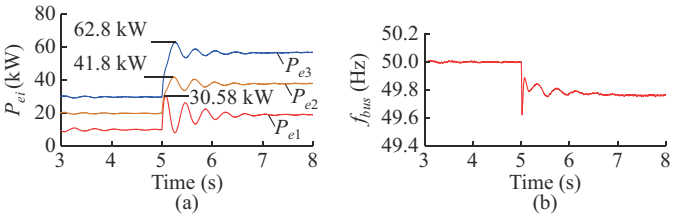

Fig. 13. Simulation results with traditional VSG control method. (a) P_{ei}. (b) f_{bus}.

Figure 14 shows the simulation results with centralized control method introduced in [10], and VSG2 suffers from a single-point communication failure at $t=7$ s. As illustrated in Fig. 14, under single communication link failure, although frequency restoration can still be achieved, serious frequency oscillation is clearly observed, and the active power sharing performances totally deteriorate.

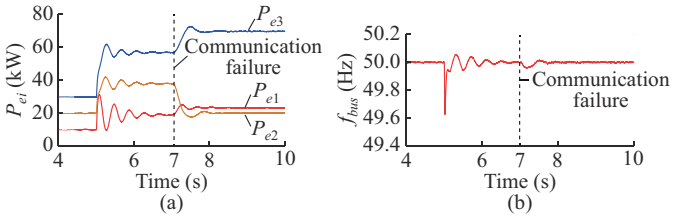

Fig. 14. Simulation results with centralize control method introduced in [10] under single communication link failure. (a) P_{ei}. (b) f_{bus}.

Figure 15 presents the simulation results with the distributed control method introduced in [11] with 60 ms communication delay. As clearly shown in Fig. 15, although both the frequency restoration and active power sharing are achieved, obvious frequency and active power oscillations occur, wherein the oscillation period is larger than 3 s, demonstrating that communication delay jeopardizes the performance of distributed control to some extent.

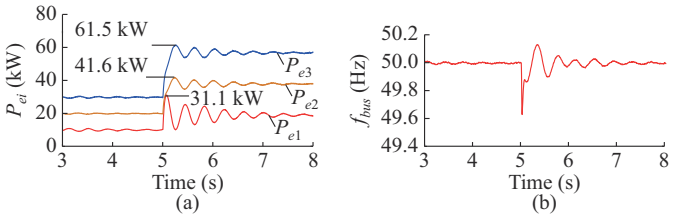

Fig. 15. Simulation results with distributed control method introduced in [11] with 60 ms communication delay. (a) P_{ei}. (b) f_{bus}.

Consequently, compared with the centralized and distributed control methods, the proposed control method exhibits significant advantages in suppressing active power oscillation while not relying on communication links, making it robust to communication failure.

The simulation results when implementing the decentralized non-error frequency regulation control method introduced in [26] are shown in Fig. 16. Although it helps achieve frequency restoration and active power sharing, active power oscillation with a large oscillatory magnitude can still be clearly observed, reflecting that the method lacks the ability to suppress active power oscillation.

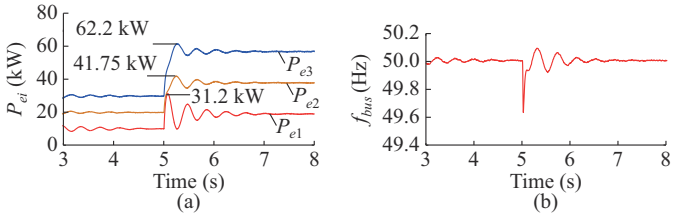

Fig. 16. Simulation results with decentralized non-error frequency regulation control method introduced in [26]. (a) P_{ei}. (b) f_{bus}.

Figure 17 shows the simulation results with the proposed control method. Compared with other control methods, under frequent load change, the proposed control method provides a satisfactory power dynamic response to load variation with a significantly smaller power oscillatory magnitude and eliminates the frequency deviation caused by load disturbance. Meanwhile, the active power sharing is well maintained. Especially, the proposed control method enjoys the advantages of a smaller overshoot magnitude and shorter settling time.

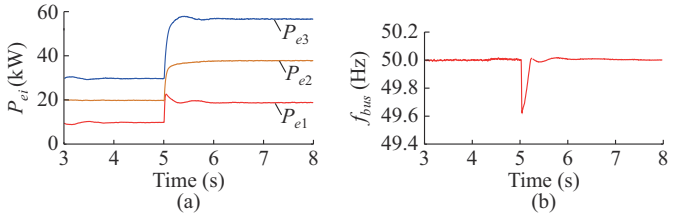

Fig. 17. Simulation results with proposed control method. (a) P_{ei}. (b) f_{bus}.

B. Case B: One VSG is Out of Service

In this case, VSG1 is assumed to malfunction and disconnect from the microgrid at $t=7$ s, and a 53 kW load is added at $t=5$ s. As observed from the results presented in Fig. 18(a), when VSG1 is out of service, the excess active power demand is shared among the remaining VSGs in a ratio of P_{e2}:$P_{e3}=2$:3, indicating the load power supplied by VSG1 is automatically allocated to the other two VSGs. As shown in Fig. 18(b), the microgrid frequency can recover to its rated value smoothly without oscillation by employing the proposed control method.

C. Case C: Plug-and-play Capability

Further investigation on the proposed control method is performed to highlight another advantage, i.e., the plug-and-play capability, as described in Fig. 19.

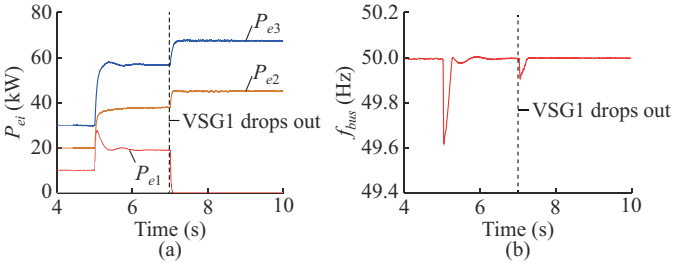

Fig. 18. Simulation results with proposed control method when VSG1 drops out. (a) P_{ei}. (b) f_{bus}.

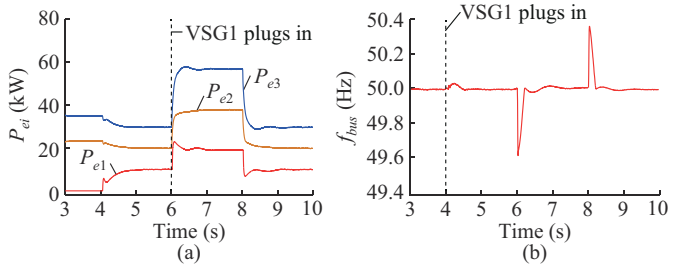

Fig. 19. Simulation results with proposed control method in plug-and-play scenario. (a) P_{ei}. (b) f_{bus}.

In Fig. 19, VSG1 is connected to the microgrid after a successful synchronization procedure [28] activated at t=4 s. In this case, a 53 kW load is added at t=6 s and removed at t=8 s. In Fig. 19(a), when VSG1 is added, the active power sharing ratio remains P_{e1}:P_{e2}:P_{e3}=1:2:3, despite frequent load changes. Besides, both the frequency restoration control and active power oscillation suppression control are effective, as shown in Fig. 19.

Moreover, it is worth noting that in the plug-and-play scenario, the proposed control method does not require any time-dependent and event-driven protocols to achieve the desired functionality.

VI. Experimental Verification

To further confirm the feasibility of the proposed control method, the experimental platform is designed and set up, which incorporates three three-phase inverters using the VSG control algorithm, as shown in Fig. 20, where DSP is short for digital signal processing, and FPGA is short for field programmable gate array. In the experiment, the key parameters and the rated capacities of different VSGs are identical to those in the simulation, and the ratio is still 1:2:3.

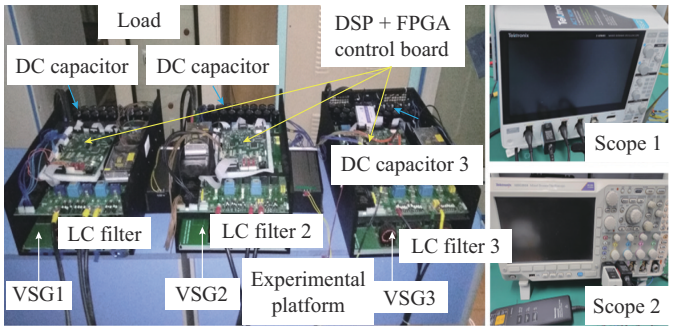

Fig. 20. Experimental platform.

A. Case A: Load Increases Suddenly

Figure 21 shows the experimental results when the load increases. The frequency is 49.98 Hz at the initial moment. When the load increases suddenly, a large frequency deviation is observed, and the frequency declines to 49.65 Hz owing to the droop mechanism. After implementing the proposed control method, the frequency deviation is eliminated. When the proposed control method is utilized, no oscillation is observed in the experimental waveforms of current at transient, and the output currents of the three VSGs always maintain a ratio of i_{o1}:i_{o2}:i_{o3}=1:2:3.

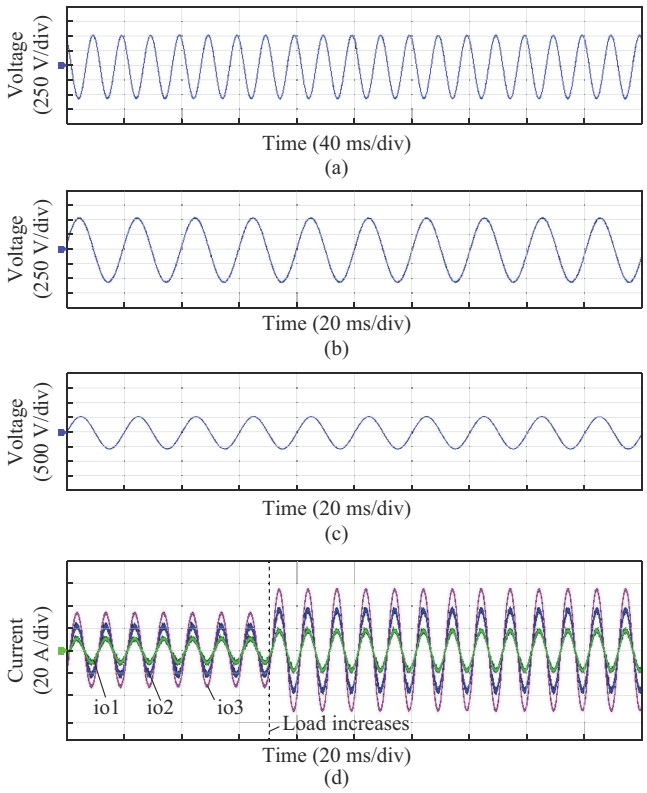

Fig. 21. Experimental results when load increases. (a) Bus line voltage at initial moment. (b) Bus line voltage when load increases without implementing proposed control method. (c) Bus line voltage when load increases after implementing proposed control method. (d) Current when load increases.

B. Case B: Load Decreases Suddenly

Figure 22 shows the experimental results when the load decreases. The steady-state frequency at the initial moment is 49.98 Hz. Without the proposed control method, the frequency deviates from its rated value and increases to 50.35 Hz when the load decreases suddenly. When the proposed control method is activated, both accurate active power sharing and frequency restoration are achieved. It should also be noted that, as described in Fig. 22(d), the output currents of the three VSGs still smoothly transition to a new steady state at a ratio of i_{o1}:i_{o2}:i_{o3}=1:2:3. In conclusion, the simulation results presented in Fig. 21 and Fig. 22 verify that the three VSGs can collectively achieve frequency recovery and proportional active power sharing simultaneously while dampening the oscillation during the transient process.

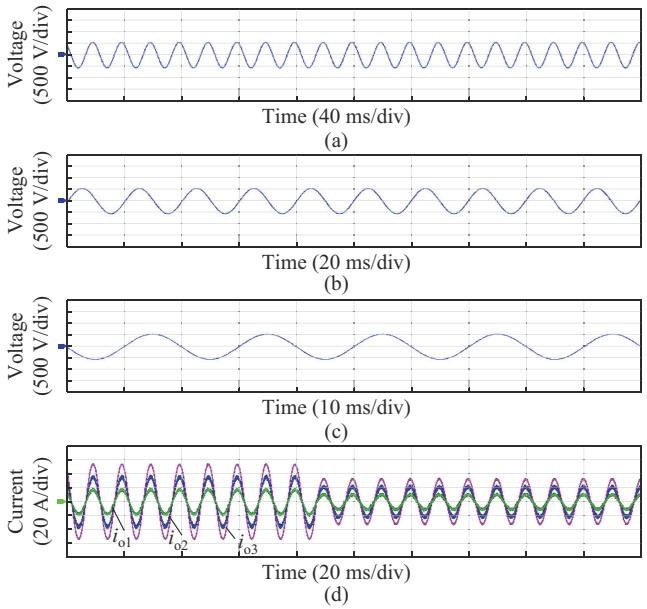

Fig. 22. Experimental result when load decreases. (a) Bus line voltage at initial moment. (b) Bus line voltage when load decreases without implementing proposed control method. (c) Bus line voltage when load decreases after implementing proposed control method. (d) Current when load decreases.

VII. Conclusion

This paper proposes a decentralized frequency restoration and power oscillation damping control method. First, the global variable characteristic of the microgrid frequency is considered to restore the microgrid frequency to its rated value, accompanied with the function of precise active power sharing. Second, by employing a transient damping enhancement module, the proposed control method can dampen power oscillation during load disturbance without affecting the system steady-state characteristic. Third, the prominent advantage of the proposed control method is that it is totally communication-free; thus, it is cost-effective, and the control performance is free from any communication failure. Moreover, straightforward design, easy implementation, and plug-and-play property are the key features of the proposed control method. This paper also provides guidelines for key control parameter design and verifies the effectiveness of the proposed control method through simulation and experiment.

References

[1] J. Dong, C. Gong, J. Bao *et al*., "Power synchronization compensation strategy based on second-order compensation links for voltage-controlled inverters in microgrids," *Journal of Modern Power Systems and Clean Energy*, vol. 11, no. 6, pp. 1935-1947, Nov. 2023.

[2] A. Fernández-Guillamón, E. Gómez-Lázaro, E. Muljadi *et al*., "Power systems with high renewable energy sources: a review of inertia and frequency control strategies over time," *Renewable & Sustainable Energy Reviews*, vol. 115, pp. 1-12, Nov. 2019.

[3] X. Meng, J. Liu, and Z. Liu, "A generalized droop control for grid-supporting inverter based on comparison between traditional droop control and virtual synchronous generator control," *IEEE Transactions on Power Electronics*, vol. 34, no. 6, pp. 5416-5438, Jun. 2019.

[4] H. Xu, C. Yu, C. Liu *et al*., "An improved virtual capacitor algorithm for reactive power sharing in multi-paralleled distributed generators," *IEEE Transactions on Power Electronics*, vol. 34, no. 11, pp. 10786-10795, Nov. 2019.

[5] J. Liu, Y. Miura, H. Bevrani *et al*., "Enhanced virtual synchronous generator control for parallel inverters in microgrids," *IEEE Transactions on Smart Grid*, vol. 8, no. 5, pp. 2268-2277, Sept. 2017.

[6] Q. Zhong and G. Weiss, "Synchronverters: inverters that mimic synchronous generators," *IEEE Transactions on Industrial Electronics*, vol. 58, no. 4, pp. 1259-1267, Apr. 2011.

[7] Z. Shuai, W. Huang, Z. Shen *et al*., "Active power oscillation and suppression techniques between two parallel synchronverters during load fluctuations," *IEEE Transactions on Power Electronics*, vol. 35, no. 4, pp. 4127-4142, Apr. 2020.

[8] M. Chen, D. Zhou, and F. Blaabjerg, "Active power oscillation damping based on acceleration control in paralleled virtual synchronous generators system," *IEEE Transactions on Power Electronics*, vol. 36, no. 8, pp. 9501-9510, Aug. 2021.

[9] C. Sun, G. Joos, S. Q. Ali *et al*., "Design and real-time implementation of a centralized microgrid control system with rule-based dispatch and seamless transition function," *IEEE Transactions on Industrial Applications*, vol. 56, no. 3, pp. 3168-3177, May 2020.

[10] T. Qian, Y. Liu, W. Zhang *et al*., "Event-triggered updating method in centralized and distributed secondary controls for islanded microgrid restoration," *IEEE Transactions on Smart Grid*, vol. 11, no. 2, pp. 1387-1395, Mar. 2020.

[11] R. Heydari, T. Dragicevic, and F. Blaabjerg, "High-bandwidth secondary voltage and frequency control of VSC-based AC microgrid," *IEEE Transactions on Power Electronics*, vol. 34, no. 11, pp. 11320-11331, Nov. 2019.

[12] N. M. Dehkordi, N. Sadati, and M. Hamzeh, "Distributed robust finite-time secondary voltage and frequency control of islanded microgrids," *IEEE Transactions on Power Systems*, vol. 32, no. 5, pp. 3648-3659, Sept. 2017.

[13] C. X. Rosero, M. Velasco, P. Martí *et al*., "Active power sharing and frequency regulation in droop-free control for islanded microgrids under electrical and communication failures," *IEEE Transactions on Industrial Electronics*, vol. 67, no. 8, pp. 6461-6472, Aug. 2020.

[14] X. Lu, X. Yu, J. Lai *et al*., "Distributed secondary voltage and frequency control for islanded microgrids with uncertain communication links," *IEEE Transactions on Industrial Informatics*, vol. 13, no. 2, pp. 448-460, Apr. 2017.

[15] M. Raeispour, H. Atrianfar, H. R. Baghaee *et al*., "Resilient $H\infty$ consensus-based control of autonomous AC microgrids with uncertain time-delayed communications," *IEEE Transactions on Smart Grid*, vol. 11, no. 5, pp. 3871-3884, Sept. 2020.

[16] M. Shi, X. Chen, J. Zhou *et al*., "Frequency restoration and oscillation damping of distributed VSGs in microgrid with low bandwidth communication," *IEEE Transactions on Smart Grid*, vol. 12, no. 2, pp. 1011-1021, Mar. 2021.

[17] Z. Li, Z. Cheng, J. Liang *et al*., "Distributed event-triggered secondary control for economic dispatch and frequency restoration control of droop-controlled AC microgrids," *IEEE Transactions on Sustainable Energy*, vol. 11, no. 3, pp. 1938-1950, Jul. 2020.

[18] Z. Lian, C. Deng, C. Wen *et al*., "Distributed event-triggered control for frequency restoration and active power allocation in microgrids with varying communication time delays," *IEEE Transactions on Industrial Electronics*, vol. 68, no. 9, pp. 8367-8378, Sept. 2021.

[19] K. Mohammadi, E. Azizi, J. Choi *et al*., "Asynchronous periodic distributed event-triggered voltage and frequency control of microgrids," *IEEE Transactions on Power Systems*, vol. 36, no. 5, pp. 4524-4538, Sept. 2021.

[20] J. Khalili, N. M. Dehkordi, and M. Hamzeh, "Distributed event-triggered secondary frequency control of islanded AC microgrids under cyber attacks with input time delay," *International Journal of Electrical Power & Energy Systems*, vol. 143, p. 108506, Dec. 2022.

[21] L. Ding, Q. Han, and X. Zhang, "Distributed secondary control for active power sharing and frequency regulation in islanded microgrids using an event-triggered communication mechanism," *IEEE Transactions on Industrial Informatics*, vol. 15, no. 7, pp. 3910-3922, Jul. 2019.

[22] Y. Khayat, M. Naderi, Q. Shafiee *et al*., "Decentralized optimal frequency control in autonomous microgrids," *IEEE Transactions on Power Systems*, vol. 34, no. 3, pp. 2345-2353, May 2019.

[23] J. M. Rey, P. Marti, M. Velasco *et al*., "Secondary switched control with no communications for islanded microgrids," *IEEE Transactions on Industrial Electronics*, vol. 64, no. 11, pp. 8534-8545, Nov. 2017.

[24] Y. Khayat, R. Heydari, M. Naderi *et al*., "Decentralized frequency control of AC microgrids: an estimation-based consensus approach," *IEEE Journal of Emerging and Selected Topics in Power Electronics*, vol. 9, no. 5, pp. 5183-5191, Oct. 2021.

[25] Y. Han, H. Li, L. Xu *et al*., "Analysis of washout filter-based power

sharing strategy – an equivalent secondary controller for islanded microgrid without LBC lines," *IEEE Transactions on Smart Grid*, vol. 9, no. 5, pp. 4061-4076, Sept. 2018.
[26] Y. Yang, P. Yang, W. Lin *et al*., "A decentralized control for non-error frequency regulation in an islanded microgrid containing multiple VSGs," *International Journal of Electrical Power & Energy Systems*, vol. 133, p. 107337, Dec. 2021.
[27] Z. Wang, Y. Chen, X. Li *et al*., "Impedance-based adaptively reshaping method for enhancing nonlinear load sharing and voltage quality in islanded microgrids with virtual synchronous generator," *IEEE Transactions on Smart Grid*, vol. 13, no. 4, pp. 2568-2578, Jul. 2022.
[28] J. Wang, N. Ramli, and N. H. A. Aziz, "Pre synchronization control strategy of virtual synchronous generator (VSG) in micro-grid," *IEEE Access*, vol. 11, pp. 139004-139016, Dec. 2023.

Xueping Li received the B.S. degree in automation from Xiangtan University, Xiangtan, China, in 2015, and the M.S. degree in electrical engineering from Hunan University, Changsha, China, in 2018. She is currently working toward the Ph.D. degree in electrical engineering from the College of Electrical and Information Engineering, Hunan University. Her research interests include microgrid, wind power generation, and wind farm optimization.

Sheng Huang received the M.S. and Ph.D. degrees both in the College of Electrical and Information Engineering, Hunan University, Changsha, China, in 2012 and 2016, respectively. He was a Postdoc with the Center for Electric Power and Energy, Technical University of Denmark, Copenhagen, Denmark, from 2017 to 2021. He is currently a Professor with the College of Electrical and Information Engineering, Hunan University. His research interests include renewable energy generation, modeling and integration of wind power, control of energy storage system, voltage control, generator, and motor control.

Zili Wang received the B.S. degree from the College of Information Engineering, Xiangtan University, Xiangtan, China, in 2015, and the M.S. and Ph.D. degrees both in electrical engineering from Hunan University, Changsha, China, in 2018 and 2023, respectively. He is currently a Postdoctoral Researcher with the College of Electrical and Information Engineering, Hunan University. His research interests include power electronics, microgrid, power quality, distributed generation, and energy storage.

Zhijie Lian received the B.S. degree in electrical engineering and automation from Huazhong University of Science and Technology, Wuhan, China, in 2017, the M.S. degree in electrical engineering from National University of Singapore, Singapore, in 2018, and the Ph.D. degree from Nanyang Technological University, Singapore, in 2023. Since May 2023, she is an Assistant Professor with the College of Electrical and Information Engineering, Hunan University. Her research interests include distributed control, smart grid, cyber-physical security, and microgrid.

Yinpeng Qu received the B.S. degree in electrical engineering and automation and the Ph.D. degree in electrical engineering from the School of Electrical Engineering and Automation, Wuhan University, Wuhan, China, in 2013 and 2021, respectively. He is currently an Associate Professor at the College of Electrical and Information Engineering, Hunan University, Changsha, China. His research interests include artificial intelligence technology, sustainable energy generation technology, and efficient operation of wind power plant.

Yandong Chen received the B.S. and M.S. degrees in instrument science and technology and the Ph.D. degree in electrical engineering from Hunan University, Changsha, China, in 2003, 2006, and 2014, respectively. He is a Professor with the College of Electrical and Information Engineering, Hunan University. His research interests include power electronics for microgrid,distributed generation, power quality, and energy storage.

Derong Luo received the M.S. and Ph.D. degrees from the College of Electrical and Information Engineering, Hunan University, Changsha, China, in 1990 and 2003, respectively. He is currently a Professor at the College of Electrical and Information Engineering, Hunan University. His research interests include permanent magnet synchronous motor drives and position sensorless control of AC motors.